

6

Measurements with Local Helioseismology

Douglas C Braun

6.1 Introduction

Local helioseismology encompasses remote observations, data analysis, and theoretical modeling of solar oscillations to infer the three dimensional structure within localized regions of the solar interior. What defines a region as “local” is relative, however, since targets of interest have included sunspots and convective elements with spatial scales $\sim 10^{-2}R_{\odot}$ as well as large-scale plasma flows spanning much of a solar hemisphere. As a relatively new discipline first explored in the 1980s, local helioseismology has two main components: first, a research component to understand the interaction of solar oscillations (acoustic and surface gravity) with perturbations within the Sun and, second, the design and application of methods to infer the properties of the perturbations by modeling the measurements of those waves. Successful applications require a thorough understanding of the physics of the waves and their interaction with inhomogeneities inside the Sun. The research component is particularly critical. For example, the types of perturbations found in the Sun can include magnetic fields for which the wave interactions can be quite complicated. Currently the types of structures most amenable to modeling using local-helioseismic measurements consist of isotropic wave-speed perturbations and the three components of plasma flows. Assessing the subsurface magnetic field directly is a challenging, but largely unrealized, goal of the field. While the status of the field is evolving, the determination of plasma flows in the first few 10s of Mm below the solar surface remains one of the primary practical applications.

We outline in this chapter the practical applications of, and resulting measurements made with, common local helioseismic methods. Broadly speaking, local helioseismology can be roughly divided into Fourier methods (which operate in the frequency wavenumber domain) and cross-covariance based methods (which oper-

ate in the space-time domain). The former (§6.3) can be considered in many ways as extensions of the analysis of global oscillations (Chapter 5) to localized regions of the Sun. Another class of methods employs cross covariance functions (§6.4) made between spatially separate signals obtained by sampling, spatial averaging or other means. These measurements are sensitive to the temporal and spatial variations of the target wave-speed perturbations and flows. For each type of method we describe the *data products* obtained through its application to remote solar observations. These products provide modelers with the raw material for inferring subsurface flows and other physical perturbations.

6.2 Geometry, projections and tracking

For many applications, local helioseismology is employed to probe solar regions spanning less than 200 Mm horizontally and extending less than a few 10s of Mm in depth. In these smaller domains one can ignore the curvature of the Sun and assume that the background medium varies only with depth z from the surface. This focus on small regions also implies that one generally considers and observes solar oscillations with smaller wavelengths (or higher degree in a spherical harmonic representation) than what is utilized in global helioseismology. In this *plane parallel approximation*, these high-degree oscillations take the form of plane waves which have a horizontal propagation described by $\exp(i[\mathbf{k}_h \cdot \mathbf{r} + \omega t])$, where \mathbf{r} is the horizontal position vector, \mathbf{k}_h is a wavevector consisting of the two horizontal components (k_x, k_y) of the wavevector, t is time, and ω is the temporal frequency. As described in Chapter 5 the stratification of the sound-speed with depth gives rise to vertical standing waves, which can be characterized by discrete values of the radial order (the number of wave nodes present in the vertical dimension). Sets of modes with the same radial order occupy parabolic-like *ridges* in the (k_h, ω) domain, where $k_h^2 = k_x^2 + k_y^2$. However, because of wave damping which increases for waves of shorter wavelength, the horizontal wavenumbers k_h of the ensemble of oscillations form a continuous set, rather than take on discrete quantum values as for global modes.

Helioseismic operations and measurements are performed on remote observations of the surface wave field ψ . The highest quality and most frequently employed observations of the wave field used in local helioseismology consist of time series, spanning hours or days, of *Dopplergrams*. These are maps of the line-of-sight velocity of the solar surface obtained either from telescopes operating in space or part of ground-based networks (see Chapter 2). Starting with observations which might span the entire observable hemisphere, a region is selected for analysis and tracked across the solar disk to remove most of the effects of solar rotation. This tracking is achieved by projecting a subset of the original image, using two-dimensional spatial interpolation, onto a local coordinate system centered on the region of interest. A

Postel’s, or azimuthal equidistant projection, is a common choice but is not exclusive in practice (e.g. Zaatari et al., 2008). Typically, the tangent point of the Postel’s projection (or other reference point) is placed at a point on the solar surface which moves with the solar rotation. Sometimes this tracking uses the Carrington rotation rate, for which the tangent point is at a fixed Carrington coordinate. But tracking rates which account for the latitudinal variation of the solar rotation may also be employed. Regardless of the rotation rate selected, it is to be understood that subsurface flows inferred from helioseismic analysis are only determined relative to this tracked rate. A three-dimensional (3D) datacube results from the time-series of projected images and forms the basis for many subsequent local helioseismic analyses.

6.3 Fourier-based methods

Spectral decomposition, through the application of Fourier transforms to the observed wave field, form the basis of several local helioseismic methods. *Hankel analysis* and *Ring-diagram analysis* use primarily transforms applied in polar and Cartesian coordinates respectively. Both methods represent the earliest applications of local helioseismic procedures and were developed to study specific solar phenomena, consisting of the scattering properties of sunspots in the former (Braun et al., 1987) and convective flows in the latter (Hill, 1988).

Because the waves sources on the Sun (believed to be caused by the turbulence of small-scale convection near the surface) are widely and randomly distributed the propagation of the resulting waves is isotropic. Thus, for a given radial order (or ridge) the power for a given wavevector k_h is distributed uniformly in all directions. If a three-dimensional Fourier transform (in two spatial dimensions and time) is performed of a tracked datacube the amplitude (or power) spectra shows a set of trumpet-like structures (see Figure 6.1). These concentric “trumpets” represent the extension into the 3D Fourier domain of of the f - and p -mode ridges.

6.3.1 Ring-diagram analysis

Ring-diagram analysis (Hill, 1988) provides a good starting point for discussing Fourier-based methods of local helioseismology. At a constant temporal frequency ω a slice through the power spectra exhibits concentric “rings” of mode power. The measurement and analysis of these spectra, collectively known as *ring-diagram analysis* seeks to determine and model the distortion of the rings due to flows and sound-speed perturbations beneath the local patch outlined by the tracked datacube.

The most common application of ring-diagram analysis has been the inference of subsurface flows. A uniform flow \mathbf{U} with horizontal components U_x and U_y relative

to the tracking rate will produce a Doppler shift of the wave frequencies, at constant \mathbf{k}_h , by an amount $\delta\omega = \mathbf{k}_h \cdot \mathbf{U} = k_x U_x + k_y U_y$. Figure 6.1 shows an example of how the rings are distorted in (k_x, k_y) space due to a horizontal flow. A more general case is when the flow varies with depth. In this case, the frequency shift is proportional to a weighted average over depth of the horizontal component of flow. The weighting is described by a *kernel function* (see Chapter 9). A uniform change (δc) to the background sound speed beneath the area of interest will expand or contract the rings independently of direction, i.e. $\delta\omega = k_h \delta c$.

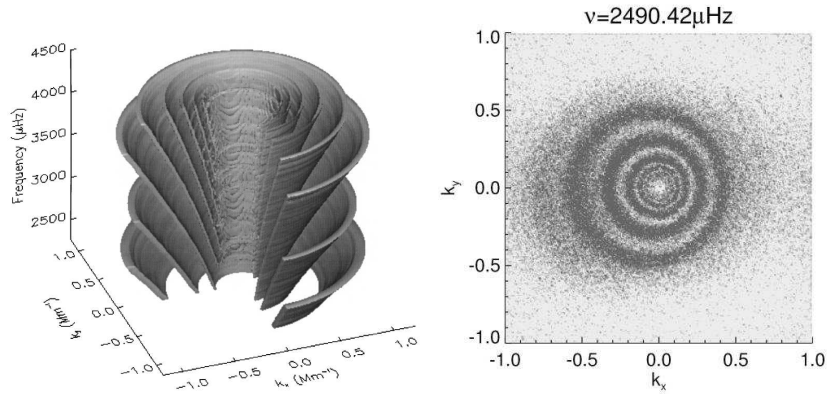


Figure 6.1 (left) a nested trumpet-like model of how the power of solar oscillations is concentrated in Fourier space. The frequency axis points upward, and the two other axes are the horizontal components of the spatial wavenumber. (From Patrón et al., 1997, and reproduced with the permission of the AAS.). (right) a slice of the 3D power spectra of actual solar observations at constant frequency showing the distortion and displacement of the rings due to a horizontal flow, in this case, due to solar rotation (figure courtesy of M. Roth).

Data products

It is the goal of ring-diagram analysis to determine, through fitting a parametrized model to the power spectra, the values of the flow parameters U_x and U_y as well as the azimuthally-averaged frequency ω_0 . A variety of models and fitting procedures have been proposed. These include directly fitting the power in the rings at slices of constant frequency (Hill, 1988; Basu and Antia, 1999). Another approach is to fit the power in cylindrical slices defined by constant horizontal wavenumber k_h (e.g. Schou and Bogart, 1998). Other parameters in the models typically include mode amplitudes and a characterization of a background term, contributed by solar convective motions and noise. Typically, Lorentzian functions are used to characterize the resonant peaks of the p -mode ridge. Asymmetries in these peaks (see Chapter 5) can be included as well (Basu and Antia, 1999).

In principal, the offset of the mean frequency ω_0 from a theoretical value computed from a solar model can help infer sound-speed perturbations. In practice, the desire to minimize systematic effects makes it advantageous to consider relative frequency shifts between a target region and one or more *reference* regions whose power spectra have been subject to identical parametrized fits.

The selection of the size of the analysis region largely determines the spatial resolution. Specifically, the horizontal resolution is essentially the diameter (sometimes called the *tile* size) of a circular mask which is typically applied to the datacube (Birch et al., 2007). The ability to resolve smaller scale flows improves with smaller tile sizes, but this happens at the cost of the ability to resolve individual p -mode ridges in the wavenumber domain, particularly at high k_h . Since the ability to infer deeper flows requires flow parameters of ridges with high wavenumber (or radial order), there is a general trade-off between horizontal resolution and depth sensitivity. Recently, progress has been made in modeling sets of tiles with multiple sizes to optimize both quantities (Featherstone et al., 2011). Historically, most ring-diagram analyses have been performed with tiles spanning about 15 degrees or smaller and which employ the plane-parallel approximation. Applications (see Chapter 13) have included the probing of a wide variety of flows in the Sun, including differential rotation, meridional (north-south) circulation, convective flows, and flows associated with sunspot groups (also known as *active regions*).

6.3.2 Fourier-Hankel and Legendre decomposition

Early, and still widely studied, targets of local helioseismology include sunspots which provide obvious localized inhomogeneities on the solar surface and have been observed visually for centuries. Arguably, the roots of local helioseismology can be found in observations and interpretations of waves inside sunspots and the accompanying theoretical analysis of wave propagation in magnetic fields (see, for example, Thomas and Weiss, 2012).

The conceptual basis for Fourier-Hankel methods (Braun et al., 1987) of local helioseismology is the assessment of waves impinging upon, and scattering from, localized perturbations like a sunspot. A cylindrical coordinate system is chosen, with the center located at the target of interest. In these (r, ϕ) coordinates, the wave equation has general solutions of the form

$$\psi(r, \phi, t) = e^{i(m\phi + \omega t)} [A_m(k_h, \omega) H_m^{(1)}(k_h r) + B_m(k_h, \omega) H_m^{(2)}(k_h r)], \quad (6.1)$$

where t is time, m is the azimuthal order, ω is the temporal frequency. A_m and B_m are the amplitudes of wave modes which have a variation in r described by Hankel functions of the first and second kind and correspond to modes propagating towards and away from the origin, respectively. Applied to observations of the solar wave field, a straightforward modification of the Hankel transform (Olver et al., 2010) which substitutes the functions $H_m^{(1,2)}$ for Bessel functions, is used to evaluate the

amplitudes A_m and B_m over the (m, k_h, ω) domain. Figure 6.2 shows sample power spectra $|A_m|^2$ and $|B_m|^2$ for a set of observations centered on a sunspot. One of the first results of this application was the discovery of absorption of incoming waves by sunspots (Braun et al., 1987).

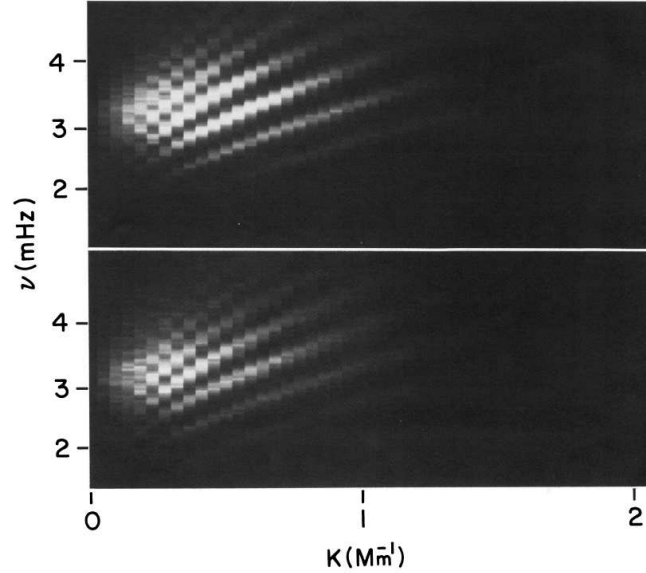


Figure 6.2 Power spectra for incoming (top panel) and outgoing (bottom panel) wave modes with respect to a target sunspot. The outgoing power is substantially reduced compared to the incoming power. (From Braun et al., 1988, reproduced with the permission of the AAS).

Some considerations on selecting the annulus size for a given temporal duration, and other details, may be found elsewhere (Braun, 1995). Analyses over large annuli, for which the curvature of the Sun can not be neglected can be performed with basis functions consisting of Legendre functions of the first and second kind (Olver et al., 2010). Obviously these methods are most effective for certain types of perturbations, typically those involving compact and isolated scatterers and which have a general azimuthal symmetry.

Data products

Absorption and emission estimates can be inferred from differences in amplitude between incoming and outgoing wave components. Phase shifts between A_m and B_m are additional parameters describing the scattering properties of the target. These shifts can be caused by refractive perturbations in the target. Observed phase shifts provided the basis for the first inferences of wave-speed perturbations below

sunspots (Fan et al., 1995). The apparent absorption seen in magnetic regions has also led to considerable theoretical study of mode conversion and simple models consistent with both absorption and phase shifts have been derived (e.g. Crouch et al., 2005). It is worth mentioning that the amplitudes determined through these methods may be affected by a variety of physical mechanisms, including absorption, a reduction of emission, and local amplitude suppression (see, e.g. Chou et al., 2009).

Mode mixing can occur when incoming wave components are scattered into different azimuthal orders or horizontal wavenumbers. Evidence of this in sunspots has been observed (Braun, 1995). However, a practical problem persists in distinguishing true mode mixing from artifacts created by the limitations of the methods or measurements. Spectral leakage is one example of this, where a finite time series or spatial size produces a spread of wave amplitude from one discrete bin of frequency or wavenumber into another.

Frequency shifts can be measured for flows beneath the annular domain. These can be determined in a manner similar to how flow parameters are determined from ridge-shifts in ring-diagram analysis. Using Legendre functions appropriate for larger regions of the solar surface, this approach has been used to probe the depth variation of meridional circulation (see Chapter 13).

6.3.3 Cross-power-spectral and Mode Coupling methods

In a local volume which is stratified vertically but uniform in the horizontal directions and in time, the Fourier wavenumber components of the wave field are uncorrelated, or in other words, independent of each other. Horizontally varying perturbations within the volume introduce a coupling of wave components of the same frequency but different horizontal wavenumbers. This implies that, in principle, perturbations can be inferred from analyses of *cross-power spectra* (e.g. Woodard, 2002). Figure 6.3 shows an example of the cross-power spectra for solar oscillation modes correlated by the presence of solar rotation and meridional circulation.

Methods for measuring mode coupling and modeling the subsurface flows have been developed and applied to a variety of problems. These include the analysis of mode coupling in a local plane-parallel approximation to deduce small-scale flows (Woodard, 2002) as well as the analysis of global spherical-harmonic modes to study meridional circulation (e.g. Schad et al., 2012). Analogous to the use of cross-power spectra to probe coupling of modes in the frequency-wavenumber domain, we discuss in the next section how local helioseismic methods using cross-covariances are used to assess correlations of the wave field directly in the space-time domain.

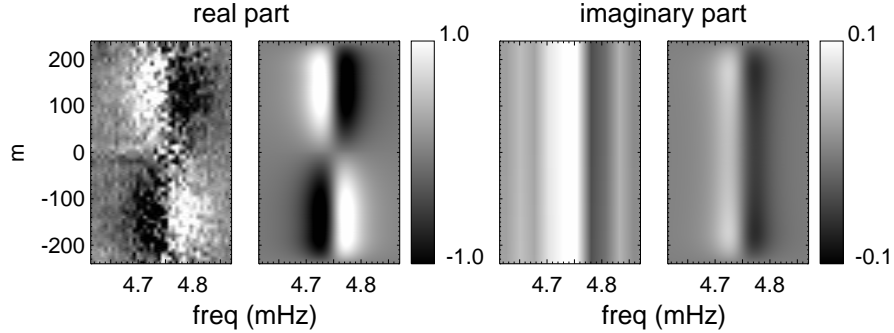


Figure 6.3 Observed and theoretical cross-power spectra for solar oscillations between spherical harmonic degree 200 and 202 and radial order $n = 8$ as a function of temporal frequency (horizontal axis) and azimuthal order m (vertical axis). The gray scale in the left and right pair of panels indicate the amplitudes of the real and imaginary part of the spectra respectively. The left (right) panel of each pair indicates the observed (theoretical model) of the cross-power spectra. The model assumes a solar-like differential rotation and meridional circulation flow. Note that the scale of the imaginary component is ten times less than the real part, and the observed imaginary component is averaged over vertical blocks in the frequency–azimuthal order domain. Figure by the author from unpublished measurements provided by M. Woodard (see Woodard, 2009, for details of the analysis)

6.4 Cross-covariance methods

6.4.1 Basic considerations

Two local helioseismic methods we focus on here are based on the cross-covariance in time between signals $\psi(\mathbf{r}_1, t)$ and $\psi(\mathbf{r}_2, t)$ at positions \mathbf{r}_1 and \mathbf{r}_2 :

$$C(\tau, \mathbf{r}_1, \mathbf{r}_2) = \int_0^T \psi(\mathbf{r}_1, t) \psi(\mathbf{r}_2, t + \tau) dt, \quad (6.2)$$

where T is the duration of the observed signals. Both time-distance helioseismology (§6.4.2) and helioseismic holography (§6.4.3), as well as the myriad flavors of these methodologies, can be defined in terms of which signals and which locations are used in the cross covariance function. The generality which unites both of these methods is that, for a wide variety of local helioseismic applications, the cross-covariance function C is used to extract *travel-time anomalies* (§6.4.4) of acoustic or surface-gravity waves propagating between the two points. By *anomalies* we mean the difference between the wave travel times in the presence of subsurface perturbations to the solar interior and the travel times without those perturbations. These travel-time anomalies can be modeled, and in many cases *inverted* (Chapter 9) to yield the subsurface structure of the perturbations, which may include wave speed changes and plasma flows. The left panel of Figure 6.4 shows an example of an averaged cross-covariance function in the (τ, Δ) domain from an application of

time-distance helioseismology to solar observations, where Δ is the distance between two points on the surface and the average is performed over many pairs of surface points.

It is helpful to understand how waves propagate between two points at the surface under the ray approximation where the wavelengths are smaller than the spatial scale of changes in the solar interior (Figure 6.4). From a starting point at the solar surface, downward propagating rays are refracted by Snell's law as the sound speed increases with depth. At a lower *turning point* the rays are horizontal and the horizontal component of the phase speed (ω/k_h) is equal to the sound speed. At the solar surface, the returning upward propagating waves are again reflected when the wavelength becomes comparable to the vertical scale of the change in the density. Deeper lower turning points are achieved by waves with greater phase speeds. Waves which do not otherwise suffer significant damping can bounce several times from the surface or even around the entire Sun.

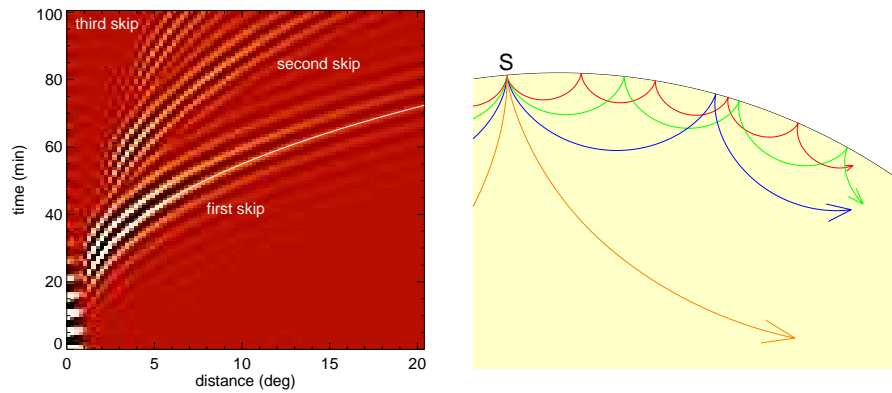


Figure 6.4 (left) A time-distance cross-covariance function in time (horizontal axis) and between samples of the wave field spaced different distances (horizontal axis) on the solar surface. The amplitude of the function, modulated by the five-minute solar oscillations, reaches maxima at times corresponding to the travel times of rays propagating through different paths of acoustic ray paths in the solar interior. (Figure by the author using unpublished cross-covariance measurements provided by T. Duvall, Jr.) (right) Ray paths of sound waves propagating downward from a specific origin S near the surface, refracting back upward to the surface, and reflecting down again to advance a number of “skips” away. (Figure by the author)

6.4.2 Time-distance helioseismology

Time distance helioseismology primarily uses the cross-covariance function between observations of the wave field sampled between two points, or averaged over patches. Frequently, the signal-to-noise is enhanced for practical purposes by using many

averages of point pairs and making the measurements over several hours or even days. The cross-covariance functions are the analog, in local helioseismology, of the seismogram in terrestrial seismology.

A common scheme employed in time-distance helioseismology is to combine cross-covariances between a point and the signal averaged over a concentric annulus (this is termed *center-annulus* geometry). In many cases, the annulus is broken up into four quadrants (Duvall et al., 1997, see Figure 6.5). *Deep-focusing* methods may also be employed, which use cross-covariance functions from signals from the opposing quadrants. In all geometries, the positive and negative time lags τ in the cross-covariance functions distinguish the travel-time anomalies for waves propagating in opposite directions. Thus, the quadrant geometry is ideal for assessing the two spatial components of directionally sensitive perturbations like flows.

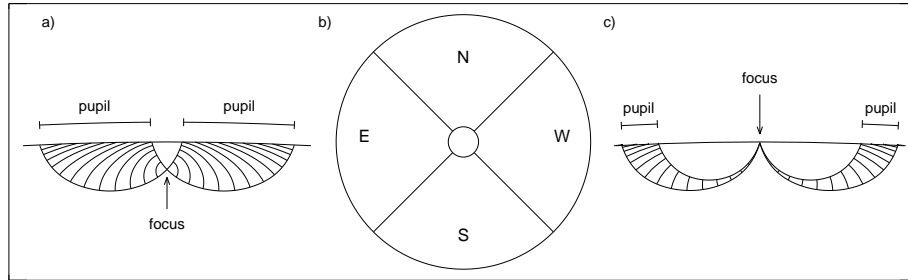


Figure 6.5 (a) the geometry employed with lateral vantage holography which selects waves which pass through a common focus point below the surface. Here the waves propagate through the focus at angles up to 45 degrees from the horizontal direction. Similar geometry is used for deep-focus time-distance methods, although frequently narrower annuli are used. (b) looking from above, the annulus used in panel (a) is divided into quadrants extending north, south, east and west on the solar surface to facilitate the assessment of the horizontal components of flows. (c) a side view of the waves selected with surface-focus methods of time-distance (also referred to as center-annulus geometry) and holography. Waves propagating from one side of the annulus bounce once at the surface focus point before reaching the other side (Figure by the author).

The cross-covariance functions in the (τ, Δ) domain made using time-distance helioseismology reveal ridge-like structures (see Figure 6.4 - these should not be confused with the p -mode ridges in the frequency-wavenumber domain). The lowest ridge (along the τ axis) corresponds to acoustic waves which reflect once from the lower turning point to arrive again at the surface a distance Δ away without additional surface reflections. At longer time lags τ , additional ridges represent the surface arrival of waves undergoing one or more skips to the surface.

Filtering

Filters are often applied to the datacube before cross-covariance methods are applied. *Phase-speed filters* are used to isolate wave modes with common ray paths

through the solar interior, and to eliminate the noise caused by unwanted contributions of other waves or by solar convective motions. These are applied to the data in the 3D Fourier domain, and usually take the form of Gaussians in the variable ω/k_h which peak at the desired phase speed and have a constant width (Couvidat and Birch, 2006).

Filters which isolate surface gravity waves (f -modes) are useful for probing inhomogeneities near the solar surface, where the energy of f -modes is concentrated. *Ridge filters* can also be employed which isolate the set of p -modes of fixed radial order. Filters in temporal frequency are also in wide use in cross-covariance methods. Typically, it is desirable to remove low frequency components of the observations which are dominated by solar convection. Filters covering narrow bands in frequency are also used in some instances. All of these filters are also commonly used in holography as well (§6.4.3). In principle, the presence and type of filter(s) used should be incorporated into the modeling and inference of the travel-time anomalies, for example, in the computation of the sensitivity functions.

6.4.3 Helioseismic Holography

Helioseismic holography (also known as computational seismic holography and ambient acoustic imaging) is a set of procedures based on phase-coherent imaging of the solar interior. Conceptually, the idea is to start with the observed wave field at the solar surface and computationally regress it, either forward or backward in time, into a solar model to estimate the amplitudes of waves propagating into and out of a remote focus point. These amplitudes are called the *ingression* H_- and *egression* H_+ (Lindsey and Braun, 2000a) and are estimated at time t and position $\boldsymbol{\rho}$ by a convolution of the surface wave field ψ with appropriate Green's functions (G_+ , G_-):

$$H_{\pm}(\boldsymbol{\rho}, t) = \int_0^T dt' \int_P d^2\boldsymbol{\rho}' \psi(\boldsymbol{\rho}', t') G_{\pm}(\boldsymbol{\rho}', \boldsymbol{\rho}, t - t'), \quad (6.3)$$

where $\boldsymbol{\rho}$ is the three-dimensional position vector and $\boldsymbol{\rho}'$ defines the solar surface. The integral in time is performed over the duration T of the observations and the integral over the surface is made over an area P called the *pupil* which is borrowed from optical terminology. The convolution expressed by Equation 6.3 is an analog, in local helioseismology, of the Kirchhoff integral theorem (e.g. Jackson, 1999). In general, Green's functions are the basic solutions to particular differential equations and are subject to the type of equations and the boundary conditions of the system. For the wave equation appropriate for the solar interior, the helioseismic holography Green's function $G_-(\boldsymbol{\rho}', \boldsymbol{\rho}, t - t')$ conceptually represents the response at the surface position $\boldsymbol{\rho}'$ and time t' due to an impulse located at position $\boldsymbol{\rho}$ and time t , while G_+ is the time-reverse of this, i.e. $G_+(\boldsymbol{\rho}', \boldsymbol{\rho}, \tau) = G_-(\boldsymbol{\rho}', \boldsymbol{\rho}, -\tau)$. These functions

regress the observed surface wave field either forwards (for G_-) or backwards (for G_+) in time and into the interior of the Sun.

One can consider a single frequency component of the wave field ψ observed at the surface $\boldsymbol{\rho}'$ by taking the Fourier transform in time of Equation 6.3. If one also restricts the analysis to a local region and assumes a plane-parallel approximation, the convolution above simplifies to

$$H_{\pm}(\mathbf{r}, z, \omega) = \int_P d^2\mathbf{r}' \psi(\mathbf{r}', \omega) G_{\pm}(|\mathbf{r} - \mathbf{r}'|, z, \omega), \quad (6.4)$$

where z and \mathbf{r} is the depth and horizontal position at which the amplitudes are to be assessed. Under these conditions it is noteworthy that the convolutions needed to compute H_{\pm} using Equation 6.4 can be performed efficiently using Fast-Fourier transforms.

To study travel-time anomalies analogous to those determined by time-distance helioseismology, one considers cross covariances between the ingressions and egression, or between either of these and the wave field ψ . For example, if the ingression and egression are both regressed, from different pupils, to some subsurface *focus* at depth z and horizontal position \mathbf{r} , then the cross-covariance of the two amplitudes can be used to determine the travel-time anomalies of waves propagating between the two pupils through the focus. This is the basis for *lateral vantage* holography (Figure 6.5), and is highly analogous to deep-focus methods in time-distance helioseismology. Other common applications include *local control correlations*, which represent the cross covariances between the surface wave field ψ with either the ingression or egression assessed over a concentric annulus, which may be divided into quadrants. This is also termed *surface-focus* holography and is analogous to center-annulus time-distance methods.

Unfortunately, the limited information available from surface Dopplergram observations requires that helioseismologist use only approximate forms of the Green's function. However, different types of Greens functions have been derived numerically using models of the solar interior under a variety of approaches and approximations. One example of their construction may be found in Lindsey and Braun (2000a). Remarkably, when the point source is located at the surface the Green's function closely resembles the time-distance cross-covariance function (e.g. Figure 6.4), which provides a conceptual linkage between holography and time-distance helioseismology.

6.4.4 Data Products

For many purposes, the travel-time anomalies, extracted from the cross-covariance functions form the main data products of interest for further modeling and inferences of the solar subsurface. However, wave excitation and absorption can be stud-

ied with egression and ingression amplitudes. Deep focus methods employing four quadrants, aligned with the cardinal directions on a region of the Sun (Figure 6.5), require the extraction of four travel time anomalies (corresponding to propagation from east to west, west to east, north to south, and south to north). Surface-focused holography and center-annulus time-distance methods use eight measurements to determine the directional components of the travel-time anomalies. In addition, sums of cross-covariance functions over the four quadrants in the annulus can be used to assess the net inward and outward travel-times. The difference of these (net outward minus inward) is sensitive to the horizontal divergence of flows and to vertical flow components. In general, the sets of measurements used for modeling flows consist of maps of the directional (east-west and north-south) travel-time differences and net (out-in) difference. The directionally averaged (or mean) travel-time anomaly is defined relative to mean travel-times computed from a solar model or (more typically) measured empirically from solar observations. This quantity is sensitive to directionally-invariant perturbations like changes in the sound speed.

A main practical difference between the cross-covariance functions determined from each method is that, in time-distance helioseismology, one extracts for further analysis the portions of the two branches of the function centered around time lags $\pm\tau$ given by the time for wave propagation between the two measurement points in the quiet Sun while, for holography, the time lag τ is near zero since the egression and ingression signals are computationally regressed towards each other in time by means of the Green's functions. There are a variety of methods to model or fit the cross-covariances to extract the travel-time anomalies and their uncertainties. Common methods include fitting cross-covariance to wavelet functions, such as the Gabor function, or to theoretical models. Couvidat et al. (2012) provides a comparison of a number of popular methods. Figure 6.6 shows some examples of maps of travel-time anomalies around a sun spot as determined from different methods.

Travel-time anomalies from cross-covariance based methods have been used to model wave-speed variations beneath active regions as well as flows on almost all spatial scales. An important application of multiple-skip cross-covariance analyses has been to map travel-time anomalies over much of the spherical solar surface, including the hemisphere on the opposite side of the Earth (Figure 6.7). This method makes use of the strong travel-time anomalies that are associated with magnetic regions which can be seen even in global oscillation modes which propagate one or more times around the Sun within their mode lifetimes. Farside imaging was first achieved with holography-based methods (Lindsey and Braun, 2000b) and subsequently with time-distance helioseismology (Zhao, 2007).

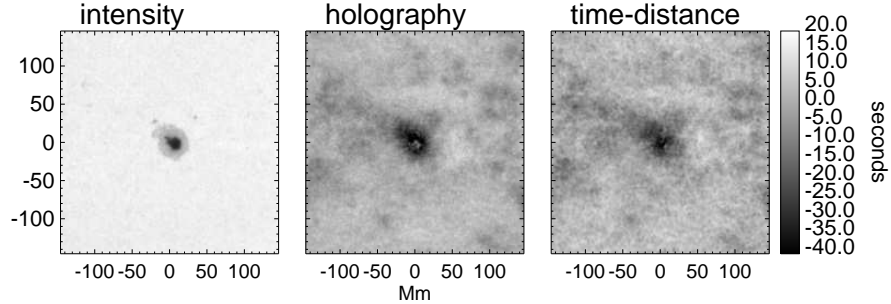


Figure 6.6 Sample maps of observed travel-time anomalies around a sunspot, employing different methods to extract the travel-times. Both maps show a decrease in travel-times within a sunspot. (Figure by the author from using measurements by the author and T. Duvall Jr.)

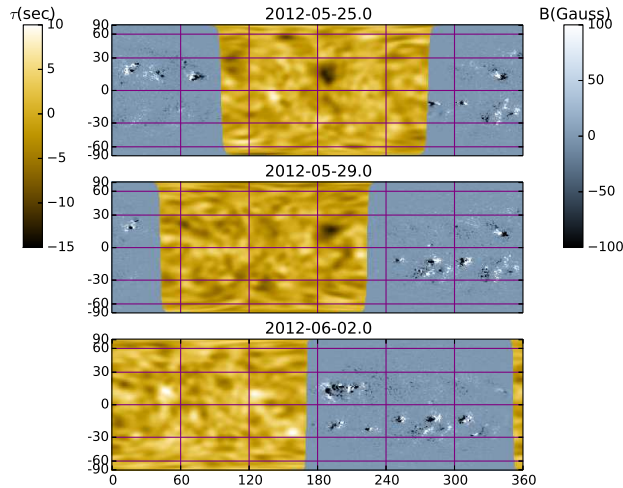


Figure 6.7 Composite far-side-seismic (left color scale) and near-side-line-of-sight magnetic maps (right grey scale) show an active region (NOAA AR11498) passing the far-side meridian (top panel) and rotating into view from earth at Carrington coordinate (190W, 13N) in the near hemisphere (bottom) in May-June, 2013. Figure provided by C. Lindsey.

6.5 Limitations and Challenges

While instrumental noise and the effects of the turbulence in the terrestrial atmosphere can affect the measurements described above, for space-based observations the main source of random errors is typically solar *realization noise* which results from the stochastic nature of the wave excitation process (e.g. Gizon and Birch, 2004). This noise provides the ultimate limits to the precision of both local and global helioseismology. While this noise can be substantially reduced by spatial and temporal averaging for some problems (e.g the probing of long-lived and large-scale

flows on the Sun), this is not practical for the study of smaller-scale flows or individual sunspots with short life-spans. Strategies that have been developed include the *ensemble averaging* of measurements which are employed to model the (averaged) properties of supergranules (Duvall and Birch, 2010) and small magnetic elements (Felipe et al., 2012).

Data products for local helioseismology, much like those for global helioseismology can be improved by long-duration observations free of the day-night duty cycle. Multiple vantage points away from the Earth-Sun line of sight, now routine for other types of solar observations, have not yet been achieved for helioseismic data and is clearly a desirable goal for future space missions. Recent theoretical developments are also facilitating the interpretation of local helioseismic data products and guiding improvements in analysis methods. For example, increasingly sophisticated magnetoconvective computations are making it possible to understand sources of systematic errors due to magnetic fields (e.g. Braun et al., 2012) and convective motions (e.g. Baldner and Schou, 2012) in the Sun.

The author is grateful for support from the NASA Heliophysics Division and from the Solar Terrestrial Program of the US National Science Foundation.

References

- Baldner, C. S., and Schou, J. 2012. Effects of Asymmetric Flows in Solar Convection on Oscillation Modes. *Astrophys. J.*, **760**, L1–L4.
- Basu, S., and Antia, H. M. 1999. Large-Scale Flows in the Solar Interior: Effect of Asymmetry in Peak Profiles. *Astrophys. J.*, **525**, 517–523.
- Birch, A. C., Gizon, L., Hindman, B. W., and Haber, D. A. 2007. The Linear Sensitivity of Helioseismic Ring Diagrams to Local Flows. *Astrophys. J.*, **662**, 730–737.
- Braun, D. C. 1995. Scattering of p-Modes by Sunspots. I. Observations. *Astrophys. J.*, **451**, 859.
- Braun, D. C., Duvall, Jr., T. L., and LaBonte, B. J. 1987. Acoustic Absorption by Sunspots. *Astrophys. J.*, **319**, L27–L31.
- Braun, D. C., Duvall, Jr., T. L., and LaBonte, B. J. 1988. The Absorption of High-degree p-Mode Oscillations In and Around Sunspots. *Astrophys. J.*, **335**, 1015–1025.
- Braun, D. C., Birch, A. C., Rempel, M., and Duvall, T. L. 2012. Helioseismology of a Realistic Magnetoconvective Sunspot Simulation. *Astrophys. J.*, **744**, 77–86.
- Chou, D.-Y., Yang, M.-H., Zhao, H., Liang, Z.-C., and Sun, M.-T. 2009. Spatial Distributions of Absorption, Local Suppression, and Emissivity Reduction of Solar Acoustic Waves in Magnetic Regions. *Astrophys. J.*, **706**, 909–916.
- Couvidat, S., and Birch, A. C. 2006. Optimal Gaussian Phase-Speed Filters in Time-Distance Helioseismology. *Solar Phys.*, **237**, 229–243.
- Couvidat, S., Zhao, J., Birch, A. C., Kosovichev, A. G., Duvall, T. L., Parchevsky, K., and Scherrer, P. H. 2012. Implementation and Comparison of Acoustic Travel-Time Measurement Procedures for the Solar Dynamics Obser-

- vatory/Helioseismic and Magnetic Imager Time - Distance Helioseismology Pipeline. *Solar Phys.*, **275**, 357–374.
- Crouch, A. D., Cally, P. S., Charbonneau, P., Braun, D. C., and Desjardins, M. 2005. Genetic magnetohelioseismology with Hankel analysis data. *Monthly Notices of the Royal Astron. Soc.*, **363**, 1188–1204.
- Duvall, Jr., T. L., and Birch, A. C. 2010. The Vertical Component of the Supergranular Motion. *Astrophys. J.*, **725**, L47–L51.
- Duvall, Jr., T. L., Kosovichev, A. G., Scherrer, P. H., et al. 1997. Time-Distance Helioseismology with the MDI Instrument: Initial Results. *Solar Phys.*, **170**, 63–73.
- Fan, Y., Braun, D. C., and Chou, D.-Y. 1995. Scattering of p-Modes by Sunspots. II. Calculations of Phase Shifts from a Phenomenological Model. *Astrophys. J.*, **451**, 877.
- Featherstone, N. A., Hindman, B. W., and Thompson, M. J. 2011. Ring-analysis flow measurements of sunspot outflows. *Journal of Physics Conference Series*, **271**(1), 012002.
- Felipe, T., Braun, D., Crouch, A., and Birch, A. 2012. Scattering of the f-mode by Small Magnetic Flux Elements from Observations and Numerical Simulations. *Astrophys. J.*, **757**, 148–160.
- Gizon, L., and Birch, A. C. 2004. Time-Distance Helioseismology: Noise Estimation. *Astrophys. J.*, **614**, 472–489.
- Hill, F. 1988. Rings and trumpets - Three-dimensional power spectra of solar oscillations. *Astrophys. J.*, **333**, 996–1013.
- Jackson, John David. 1999. *Classical electrodynamics*. 3rd edn. New York, NY: Wiley.
- Lindsey, C., and Braun, D. C. 2000a. Basic Principles of Solar Acoustic Holography. *Solar Phys.*, **192**, 261–284.
- Lindsey, C., and Braun, D. C. 2000b. Seismic Images of the Far Side of the Sun. *Science*, **287**, 1799–1801.
- Olver, F. W., Lozier, D. W., Boisvert, R. F., and Clark, C. W. 2010. *NIST Handbook of Mathematical Functions*. New York, NY, USA: Cambridge University Press.
- Patrón, J., González Hernández, I., Chou, D.-Y., Sun, M.-T., et al. 1997. Comparison of Two Fitting Methods for Ring Diagram Analysis of Very High L Solar Oscillations. *Astrophys. J.*, **485**, 869–874.
- Schad, A., Timmer, J., and Roth, M. 2012. Measuring the solar meridional flow from perturbations of eigenfunctions of global oscillations. *Astronomische Nachrichten*, **333**, 991–994.
- Schou, J., and Bogart, R. S. 1998. Flow and Horizontal Displacements from Ring Diagrams. *Astrophys. J.*, **504**, L131–L134.
- Thomas, J. H., and Weiss, N. O. 2012. *Sunspots and Starspots*. New York, NY, USA: Cambridge University Press.
- Woodard, M. F. 2002. Solar Subsurface Flow Inferred Directly from Frequency-Wavenumber Correlations in the Seismic Velocity Field. *Astrophys. J.*, **565**, 634–639.
- Woodard, M. F. 2009. Helioseismic Measurement of Large-Scale Solar Flows. in *Solar-Stellar Dynamos as Revealed by Helio- and Asteroseismology: GONG 2008/SOHO 21*, ed. Dikpati, M., Arentoft, T., González Hernández, I., Lindsey, C., and Hill, F. Astronomical Society of the Pacific Conference Series, 416.

- Zaatri, A., Corbard, T., Roth, M., González Hernández, I., and von der Lühe, O. 2008. Comparison of geometrical mapping for ring diagram analysis. *Journal of Physics Conference Series*, **118**(1), 012090.
- Zhao, J. 2007. Time-Distance Imaging of Solar Far-Side Active Regions. *Astrophys. J.*, **664**, L139–L142.